Polymer 51 (2010) 4127–4139

Contents lists available at ScienceDirect

Polymer

journal homepage: www.elsevier.com/locate/polymer

Biodegradable self-reporting nanocomposite films of poly(lactic acid) nanoparticles engineered by layer-by-layer assembly

Victor H. Orozco [a,b,1], Veronika Kozlovskaya [a,1], Eugenia Kharlampieva [a], Betty L. López [b], Vladimir V. Tsukruk [a,*]

[a] School of Materials Science and Engineering, Georgia Institute of Technology, Atlanta, GA 30332, USA
[b] Grupo Ciencia de los Materiales, Universidad de Antioquia, Calle 62 52 59 Medellín, Antioquia, Colombia

ARTICLE INFO

Article history:
Received 25 April 2010
Received in revised form
18 June 2010
Accepted 30 June 2010
Available online 8 July 2010

Keywords:
Biodegradable
Layer-by-layer composite films
Poly(D,L-lactic acid) particles

ABSTRACT

We designed and fabricated multilayer assemblies of biodegradable poly(lactic acid) (PLA) nanoparticles based on hydrogen-bonding or electrostatic interactions. The PLA nanoparticles were prepared by precipitation method and their surface charge was switched by modified precipitation in the presence of poly(ethylene imine) (PEI). Moreover, gold nanoparticles were grown within the PLA nanoparticle assemblies either through UV-irradiation or under mild reducing conditions to create biodegradable nanocomposites with distinct optical response which allows monitoring biodegradation of the films. The nanocomposite coatings of PLA nanoparticles were enzymatically degraded by α-chymotrypsin. We demonstrated that the biodegradation process can be colorimetrically monitored with UV–vis spectroscopy thus opening the way for facile and real-time monitoring useful for biotechnology applications.

1. Introduction

Ultra-thin (below 100 nm) polymer films present a great interest relevant for nanotechnology due to their useful functions such as high flexibility, controlled permeability, conformal nanocoating, and light transparency [1–4]. Combining ultra-thin polymer films with nanoparticle fillings provide the novel hybrid materials with important physical properties such as high strength modulus, and optical functionalities for synergistic characteristics from the initial constituents [5–7]. Ultra-thin functional nanocomposite films have been finding many applications in the fields of integrated optics, pressure and chemical sensing, reinforcement, and biosensing [8–18]. Fabrication of ultra-thin films based on polymer colloids is promising as aqueous dispersions of pH-, temperature-sensitive microparticles can be prepared [19]. Moreover, the polymer particles allow the higher surface areas compared to a polymer monolayer and can be used as microreactors for noble metals, semiconductors, and biominerals relevant for designing materials with advanced properties [20–22].

Layer-by-layer assembly (LbL), which is one of the facile approaches for assembling ultra-thin films, provides arrangement of polymers and vS200arious constituents with a precise control over structural organization of multilayers [23]. Ionic [23–27], hydrogen-bonding [28,29] and covalent interactions [30,31] are the main driving forces for building up conformal multilayer coatings on chemically and geometrically diverse substrates. Importantly, hydrogen-bonding offers fabrication of nanocoatings in biologically and physiologically relevant pH range under mild environmental conditions. Moreover, the hydrogen-bonded LbL assembly of films and shells in water allows incorporating uncharged biocompatible polymers or poorly charged functional molecules within the LbL structures [28,32]. The LbL fabrication allows a simple control over the total film thickness from few nanometers to several micrometers by increasing the number of deposited layers [33–39].

Poly(lactic acid) (PLA), a prospective component for biodegradable LbL films, is biocompatible, biodegradable and can provide mechanical strength to a thin film in the absence of degrading conditions [40–43]. PLA and its copolymers with poly(glycolic acid) (PLGA) have been widely used for nanoparticle synthesis for drug delivery or controlled administration of different therapeutic agents [44–49]. PLA particles, fibers and films have been demonstrated relevant for biomedical field. For example, PLA nanoparticles with avidin-modified surfaces have been reported for diagnostic and therapeutic applications [50]. Films of PLA copolymers or composites cast from organic solvents have been used as substrates for cell culturing [51,52]. PLA nanoparticles as a component for LbL films can be prepared as solid or hollow nano- or micro-spheres [53–57].

* Corresponding author.
E-mail address: Vladimir@mse.gatech.edu (V.V. Tsukruk).
[1] The authors equally contributed to this work.

0032-3861/$ – see front matter © 2010 Elsevier Ltd. All rights reserved.
doi:10.1016/j.polymer.2010.06.060

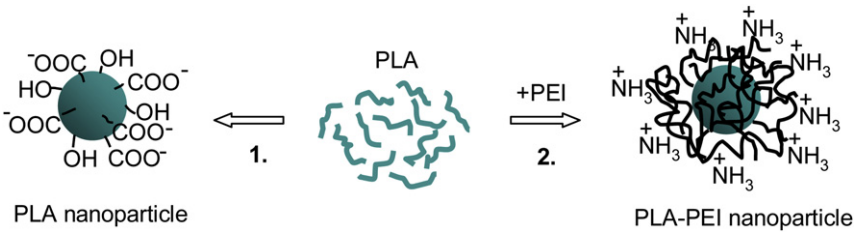

Scheme 1. Schematic representation for preparation of bare PLA (1) and cationic PLA–PEI nanoparticles (2) by precipitation of PLA polymer from acetone into aqueous solutions.

Despite the useful degradability function of PLA, concerns have been expressed that the lack of PLA surface charges can prevent it from being used for assembling into robust ultra-thin films with polyelectrolytes by regular LbL assembly [58]. Nevertheless, Akashi and co-workers demonstrated the LbL assembly of PLA polymer and poly(L-lysine) or poly(diallyldimethylammonium chloride) through extremely weak ion–dipole interactions [58]. Moreover, it has been shown that solvents used for preparation of PLA nanoparticles determine the surface properties of the PLA nanoparticles which eventually might make them suitable for LbL assembly [59]. For example, PLA nanoparticles prepared from chloroform can be coated with polyelectrolytes such as poly(allylamine hydrochloride)–poly(styrene sulfonate) (PAH–PSS) layers through membrane filtration approach [59]. After being coated with 3 bilayers of PAH/PSS, the PLA nanoparticles exhibited lower aggregation tendency in aqueous solution due to the increased surface hydrophylicity because of the formed coating.

Embedding gold nanoparticles into polymer matrices can be an effective way to add unique optical properties to ultra-thin polymer films as well as make them mechanically robust and susceptible to heat [60–62]. In-situ nanoparticle synthesis within the multilayer polymer films can be used to obtain gold nanoparticles in a controlled manner due to the confined environment of the polyelectrolyte multilayers allowing a precise control over nanoparticle shapes, morphologies and sizes. Polyelectrolyte multilayers have been rarely reported to serve as nanoreactors for nanoparticles synthesis. For example, PSS/PAH films were shown to generate free amino groups to attach tetrachloroaurate ions for gold reduction after the polymer assembly was exposed to particular extreme pH conditions [63]. We have recently reported on the

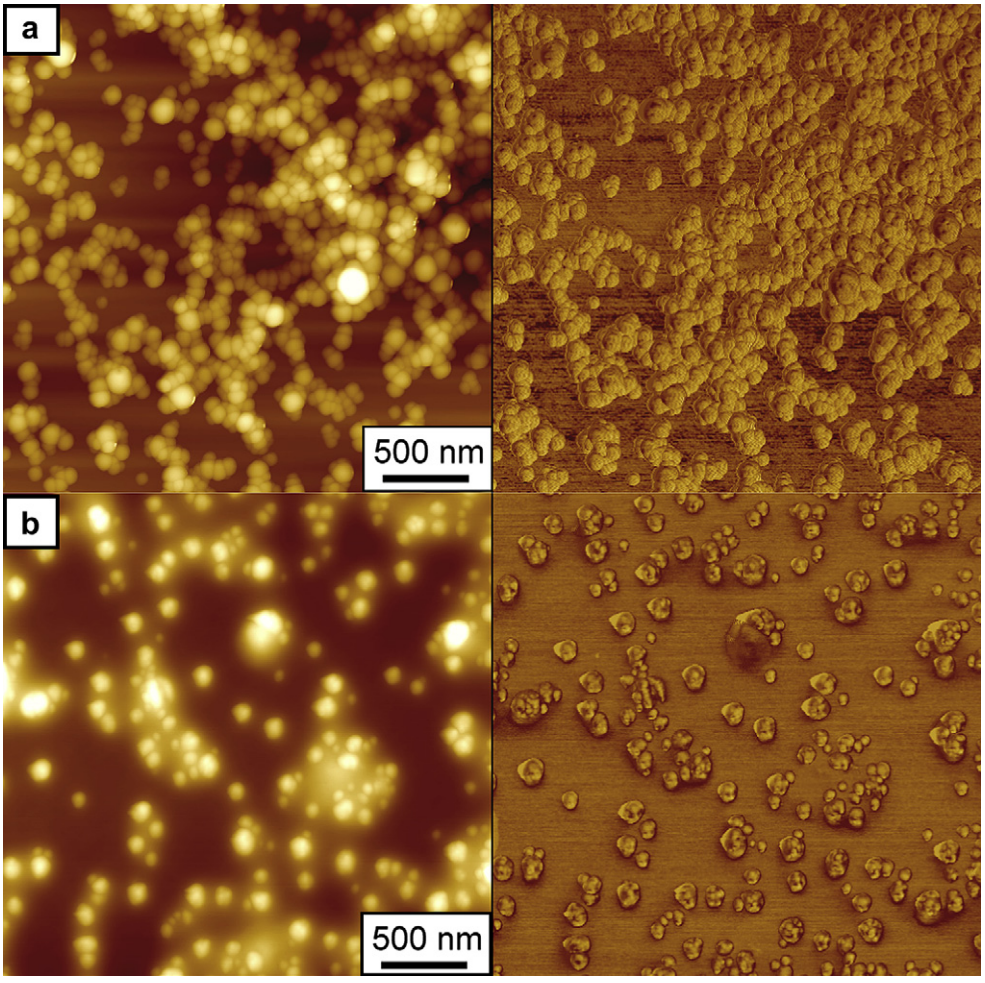

Fig. 1. AFM topography (left) and phase (right) images of bare PLA (a) and cationic PLA–PEI (b) nanoparticles drop-cast from aqueous dispersions on a surface of silicon wafers.

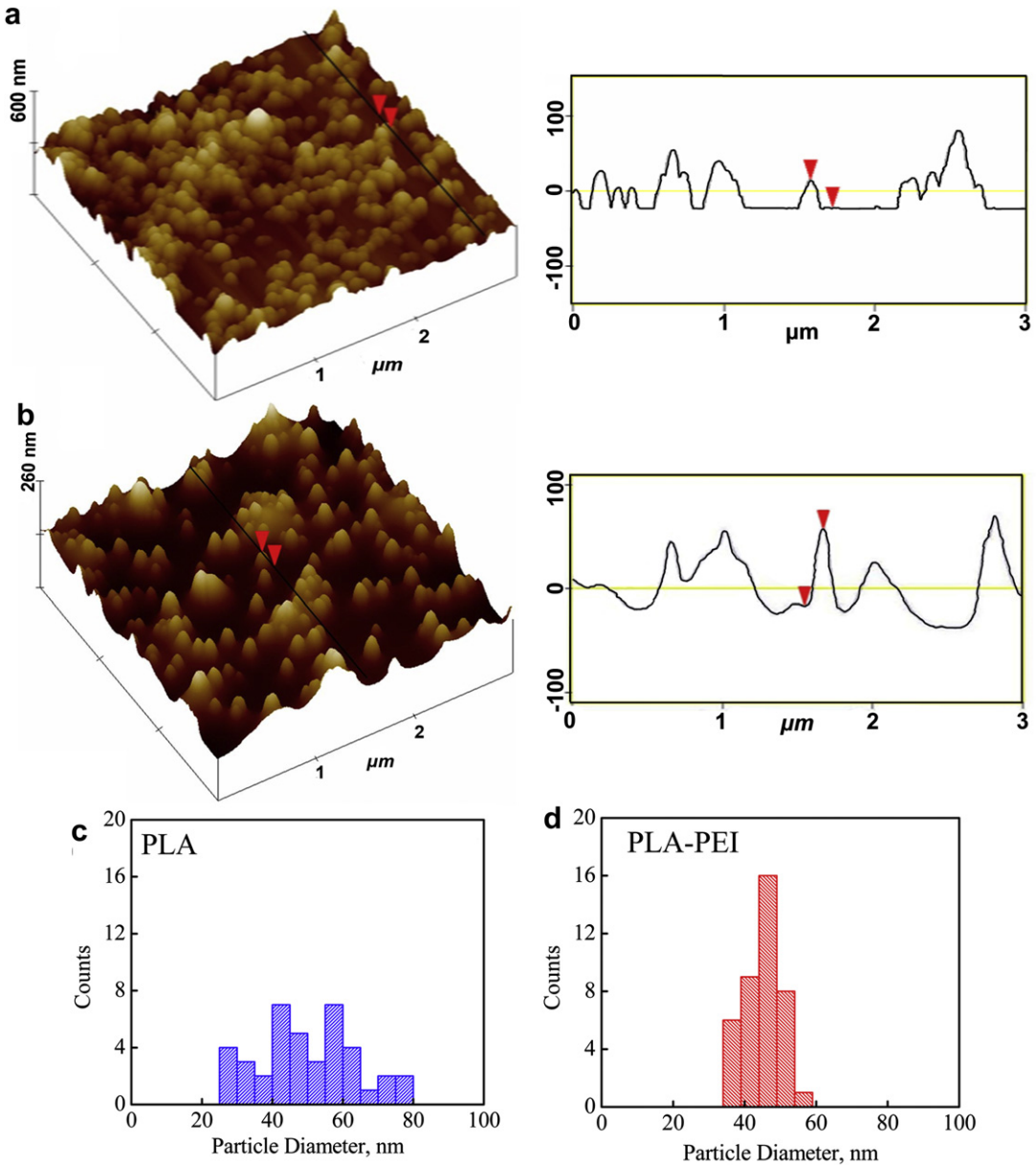

Fig. 2. 3D AFM views and cross-section analysis of bare PLA (a) and modified PLA–PEI (b) nanoparticles with their size histograms (c and d, respectively).

utilization of free amine groups within pH-responsive layered hydrogels as binding sites for gold anions within the multilayer films, otherwise difficult to realize [64].

In this study, we explored possibilities of assembling PLA nanoparticles into ultra-thin films with biodegradable properties via the LbL assembly. We applied the spin-assisted LbL assembly of PLA nanoparticles on planar substrates using either hydrogen-bonding or ionic interactions. The hydrogen-bonded PLA/poly (vinylpyrrolidone) (PLA/PVPON) LbL assembly was studied under various pH conditions and we found that these films can be fabricated only at highly acidic conditions, i.e. at pH < 3. The cationic PLA nanoparticles synthesized in presence of poly(ethylene imine) (PLA–PEI) were LbL-assembled with poly(acrylic acid) (PAA) and later cross-linked for robustness. Importantly, the produced hydrogen-bonded assemblies of PLA/PVPON possess a unique pH-stability in the pH range from pH 2 to pH 10. We suggest that this stability is caused mostly by hydrophobic interactions between PLA nanoparticles.

Moreover, fine gold nanoparticles were successfully grown within the PLA nanoparticle coatings due to present or introduced free amine groups. We demonstrate that the reduced gold nanoparticles can be used for optical report of changes within the assemblies associated with enzymatically induced degradation of the PLA nanoparticle films by α-chymotrypsin. In contrast to planar assemblies, only PLA–PEI particles were able to form conformal coatings through ionic interactions on particulate substrates (silica particles), to yield free-standing hollow shells of $(PLA–PEI/PAA)_n$. We explored amine functionalities present in the shells for the reduction of gold nanoparticles within the shells via either UV-initiated reduction or under mild conditions without a reducing agent. We found that unlike the UV-based reduction, the later method is able to produce stable gold-containing PLA nanoshells with plasmonic properties which can be utilized for self-reporting of biodegradation.

We suggest that ultra-thin polymer films can be useful in bionanotechnology in applications related to functional delivery if

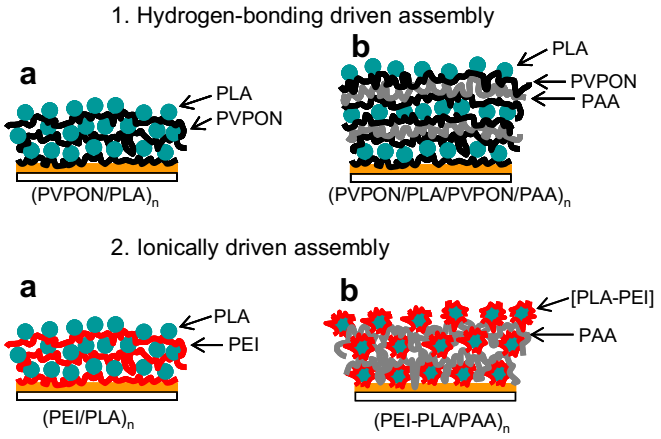

Scheme 2. Schematic representation of PLA nanoparticle assemblies through hydrogen-bonding (1) or ionic interactions (2).

biodegradable components are exploited for their fabrication. They can respond to degrading surroundings promoting a controlled delivery process, and wherein the release will depend on breakdown of the assembly due to biodegradability of the formed polymer films with PLA component.

2. Experimental section

2.1. Materials

The poly-(D,L-lactic acid) (PLA $M_n = 136{,}000$) of injection grade was supplied by Jamplast Inc (Ellisville, USA), PAA ($M_w = 90{,}000$), PVPON ($M_w = 55{,}000$), poly(ethylene imine) (PEI $M_w = 70{,}000$, 30% aqueous solution), mono- and dibasic sodium phosphate, 1-ethyl-3-(3-dimethylaminopropyl) carbodiimide hydrochloride (EDC), ethylene diamine (EDA), $HAuCl_4$ solution were purchased from Sigma–Aldrich. Acetone and 0.1 M borate buffers (pH 10) were received from J.T. Baker. Ultrapure water with a resistivity of 18.2 MΩ cm was used (Nanopure system). Silica microspheres with the average size of 4 microns were from Polysciences Inc. Quartz microscope fused slides (Alfa Aesar) and single-side polished silicon wafers of the [100] orientation (Semiconductor Processing

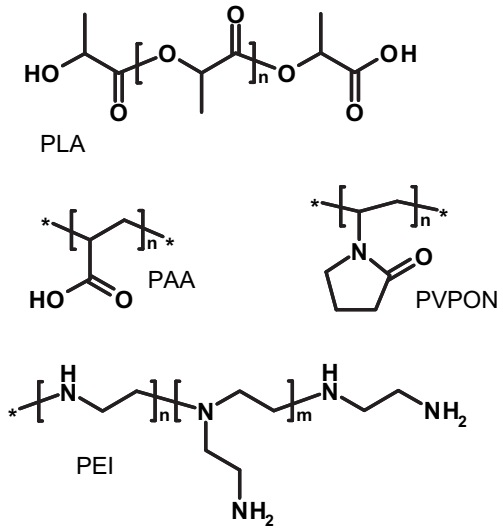

Scheme 3. Chemical structures of poly(lactic acid) (PLA), poly(N-vinylpyrrolidone) (PVPON), poly(acrylic acid) (PAA), poly(ethylene imine) (PEI).

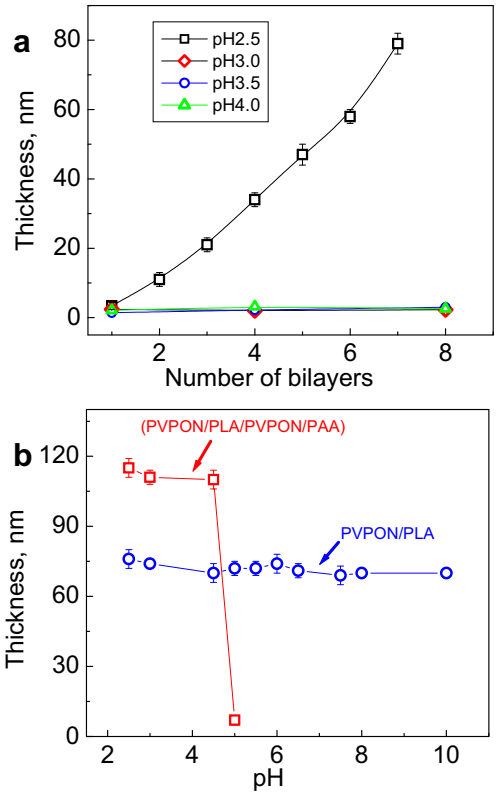

Fig. 3. Assembly of PVPON/PLA LbL films at various pH values (a). pH-stability of $(PVPON/PLA)_8$ (circles) and $(PVPON/PLA/PVPON/PAA)_8$ (squares) at various pH conditions (b).

Co.) were cut by typical size of 10 × 20 mm and cleaned in a piranha solution as described elsewhere [13].

2.2. PLA nanoparticles fabrication

PLA nanoparticles were prepared using acetone as a solvent for PLA [65]. Bare and PEI-coated PLA nanoparticles (PLA–PEI) were prepared for this study [59]. Bare PLA nanoparticles were prepared according to the following procedure [65]. 40 mg of PLA polymer were first dissolved in 8 mL of acetone. The organic solution was poured in 16 mL of de-ionized water by using a syringe under moderate magnetic stirring. The aqueous phase immediately turned white. The acetone, which rapidly diffused towards the aqueous phase, was evaporated by continuous stirring during 24 h inside a laboratory hood under reduced pressure, and the aqueous phase became opalescent due to formation of the nanoparticles. The polycation-coated PLA nanoparticles were prepared by dissolving 40 mg of PLA in 10 mL of acetone. The resulting organic solution was poured in 22 mL of 2.0 mg/mL PEI aqueous solutions at pH 6.8 using a syringe and under moderate magnetic stirring. The PLA–PEI nanoparticles for assembly on silica particles were also prepared in the presence of 0.5 mg/mL and 0.2 mg/mL solutions of PEI.

2.3. Fabrication of LbL assemblies of PLA nanoparticles

Hydrogen-bonded $(PVPON/PLA)_8$ planar assemblies were formed by spin-assisted LbL (SA-LbL) [66,67]. Briefly, two bilayers of PEI/PAA were deposited from 0.01 M buffer solutions with polymer concentration of 2.0 mg/mL on silicon wafers or quartz slides at pH 5.0 to ensure the adhesion of the following layers. Then the $(PEI/PAA)_2$ films were heated to 175 °C for 1 h in an oven for

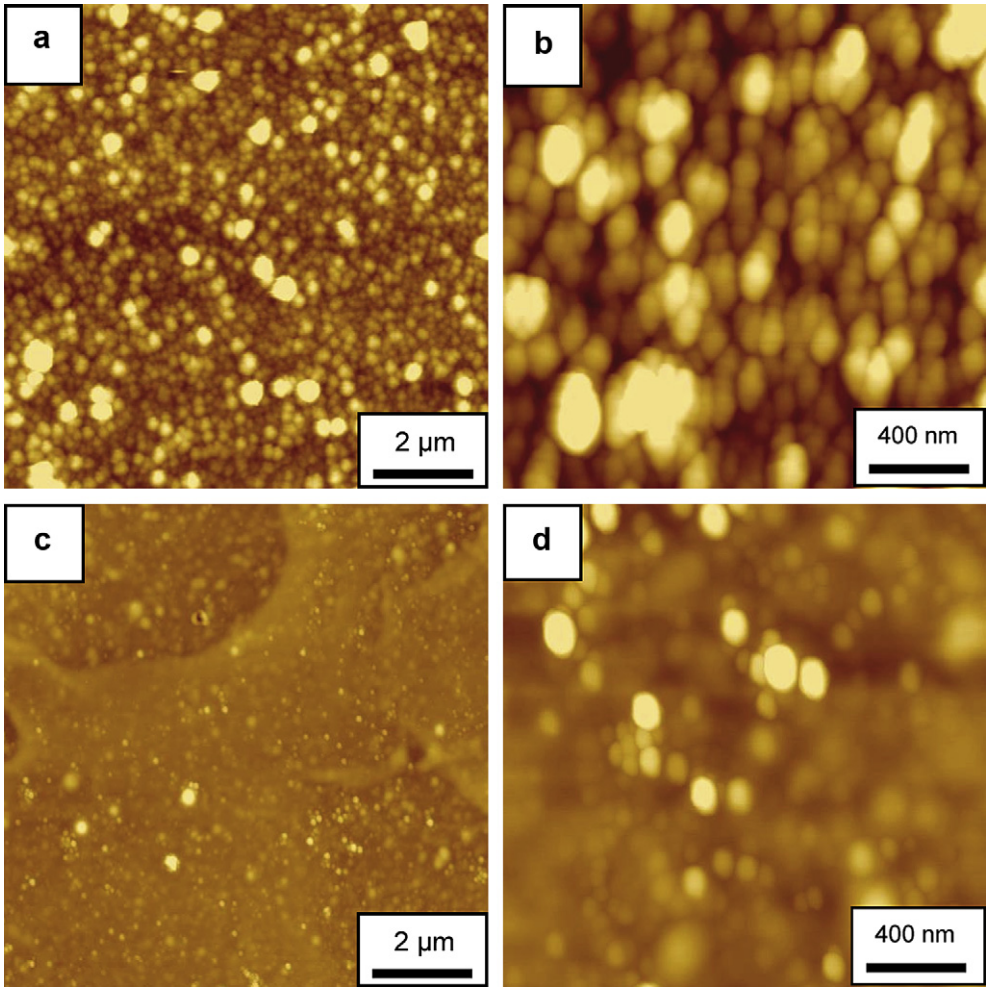

Fig. 4. AFM topographical images of the hydrogen-bonded $(PVPON/PLA)_8$ (a, b) and $(PVPON/PLA/PVPON/PAA)_8$ (c, d) LbL films. Z-scale is 150 nm (a, c) and 70 nm (b, d), after cross-linking.

thermal cross-linking of amino groups of PEI and carboxylic groups of PAA [68].

Hydrogen-bonded PVPON/PLA LbL films were assembled on top of the pre-layers. The concentration of PVPON solution was 2.0 mg/mL and its pH was adjusted with 0.1 M aqueous solution of HCl. Concentration of the PLA nanoparticle dispersion was 2.5 mg/mL. The SA-LbL of PVPON and the PLA nanoparticles onto the substrates was performed at 4000 rpm for approximately 30 s per deposition step, starting from PVPON and followed by two rinsing steps with 0.01 M phosphate buffer at certain pH. The final configuration of the PLA nanoparticle assembly can be presented as $(PEI/PAA)_2/(PVPON/PLA)_8$ were the subscripts denote the number of deposited bilayers (Scheme 2.1a).

After hydrogen-bonded multilayers were formed, the PLA nanoparticles were chemically cross-linked with ethylene diamine (EDA) to introduce free amine groups within the films. For that, surface-tethered $(PEI/PAA)_2/(PVPON/PLA)_8$ films were immersed into 5 mg/mL solution of EDC at pH 5.0 for 30 min to activate the carboxylic groups of PLA nanoparticles. After washing in phosphate buffer at pH 5, the substrate-tethered films were transferred into 5 mg/mL EDA solution at pH 5.0 for 16 h to introduce amide linkages between EDA molecules and the activated carboxylic groups of PLA [69].

Ionically interacted multilayers of $(PEI/PLA)_8$ were fabricated using the procedure described above, with the $(PEI/PAA)_2$ pre-layers deposited in the same way described above (Scheme 2.2a). The concentrations of PEI buffer solutions were 2 mg/mL with pH adjusted to 5. The SA-LbL process was performed using the same speed and rotation time as mentioned above. The LbL films of PEI-coated PLA nanoparticles (PLA–PEI) were fabricated at pH 6.8 using 2 mg/mL PAA solution (Scheme 2.2b). Covalent cross-linking was performed by exposure of the (PLA–PEI/PAA) films to carbodiimide solution to introduce amide linkages between carboxylic groups of PLA nanoparticles or PAA and amine groups of PEI.

Deposition of the PLA nanoparticle layers on spherical substrates was conducted as described previously [28]. PLA nanoparticle stacks were fabricated using the centrifugation method with the two bilayers of PEI/PAA deposited first. The concentrations of PEI and polyacid solutions were 2 mg/mL in TRIS buffer (Sigma) at pH 6.0. Fabrication of $(PLA–PEI/PAA)_4$ LbL coatings followed at pH 6 using 2 mg/mL polyacid solution. Covalent cross-linking was performed by exposure of the $(PLA–PEI/PAA)_4$ core-shells to carbodiimide solution for amide linkages between carboxylic groups of PLA nanoparticles or polyacid and amine groups of PEI. For hollow shells, silica templates were etched away in 8% aqueous HF solution for 8 h. The dispersion of the resultant shells was dialyzed against de-ionized water for 2 days.

2.4. Growth of gold nanoparticles within PLA nanoparticle films

Two methods were used for reduction of gold nanoparticles within the PLA nanoparticle coatings. In the first method, the quartz-tethered PLA nanoparticle coatings were exposed to 10 mL

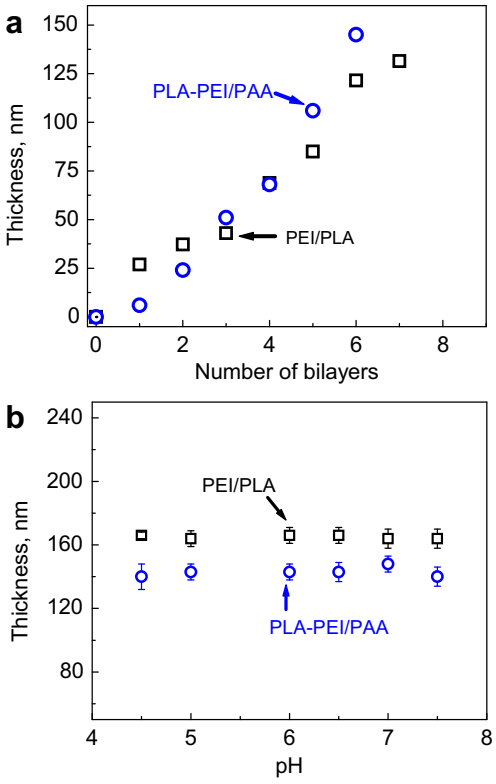

Fig. 5. The spin-assisted LbL growth of (PLA–PEI/PAA) (circles) and (PEI/PLA) coatings (squares) (a) and their pH-stability (b).

of 1.6 mM $HAuCl_4$ solution in 0.1 M borate buffer (pH 10) for 2 h, or to 2 mL of 5 mM $HAuCl_4$ solution in 0.1 M borate buffer overnight in case of core-shells, rinsed with borate buffer and left in buffer for 48 h in the dark [64]. After that, the quartz slides or core-shell solutions were rinsed with the borate buffer followed by rinsing with de-ionized water. Finally, the coatings were dried and their UV–visible absorbance spectra were recorded.

In the second method, UV-induced reduction was used to produce gold-containing PLA nanoparticle coatings [63]. In this approach, films or core-shells were subjected to $HAuCl_4$ solutions (5 mM) at pH 2.5 in the dark for 15 min, followed by three rinsing steps with water. After being dried at room temperature, the planar samples were irradiated with UV light, 365 nm, (Blak-Ray UVP, Model B-100A), for 24 h [63]. Core-shell suspensions were directly exposed to the UV-irradiation.

2.5. Film biodegradation

The degradation procedure is based upon biodegradation tests adapted for polyesters [70–77]. Specifically, for biodegradation experiments, enzymatic degradation was carried out in a 30 mL vial by dipping the slide in 10 mL of 1.0 mg/mL α-chymotrypsin (0.1 M NaCl in 0.1 M phosphate buffer at pH 7.5). Degradation was carried out at 36 °C with the enzyme solution changed every 24 h and UV spectra were recorded periodically.

2.6. Characterization

Molecular weights were determined using gel permeation chromatography on a Waters-2414 instrument with the refractive index detector. PLgel 5 μm Mixed-C column was pumped with 1.0 mL/min tetrahydrofuran at 30 °C.

The ζ-potential measurements of PLA nanoparticle dispersions were performed on a DT 300 equipment (Dispersion Technology) using the electroacoustic colloidal vibration current technique (CVI). The default frequency was 3 MHz ζ-potential measurements were performed in aqueous phase at pH = 6.5 and the average values were obtained by averaging ten independent measurements.

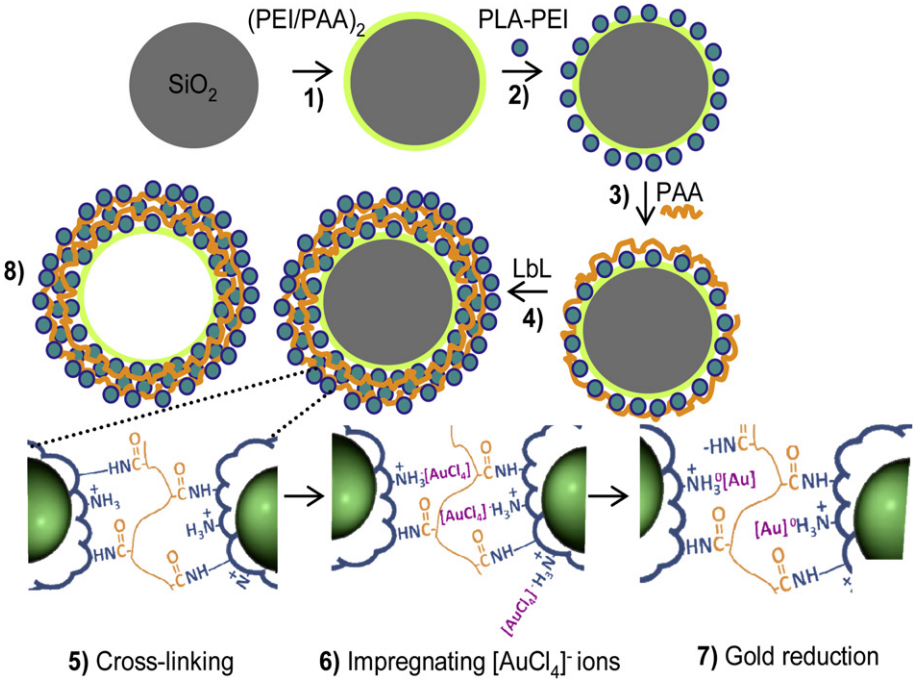

Scheme 4. Fabrication of PLA nanoparticle core-shells and hollow shells: (1) Silica particles are modified with $(PEI/PAA)_2$ pre-layers, (2) PLA–PEI nanoparticle layer is deposited on the silica templates, (3) PAA layer is ionically assembled on top of PLA–PEI nanoparticle layer, (4) deposition of (PLA–PEI/PAA) multilayers, (5) cross-linking of PLA–PEI and PAA layers, (6) impregnation of gold precursor ions within the coatings, (7) reduction of gold ions to gold nanoparticles in borate buffer at pH = 10, (8) etching silica cores to yield hollow $(PLA–PEI–Au/PAA)_n$ shells.

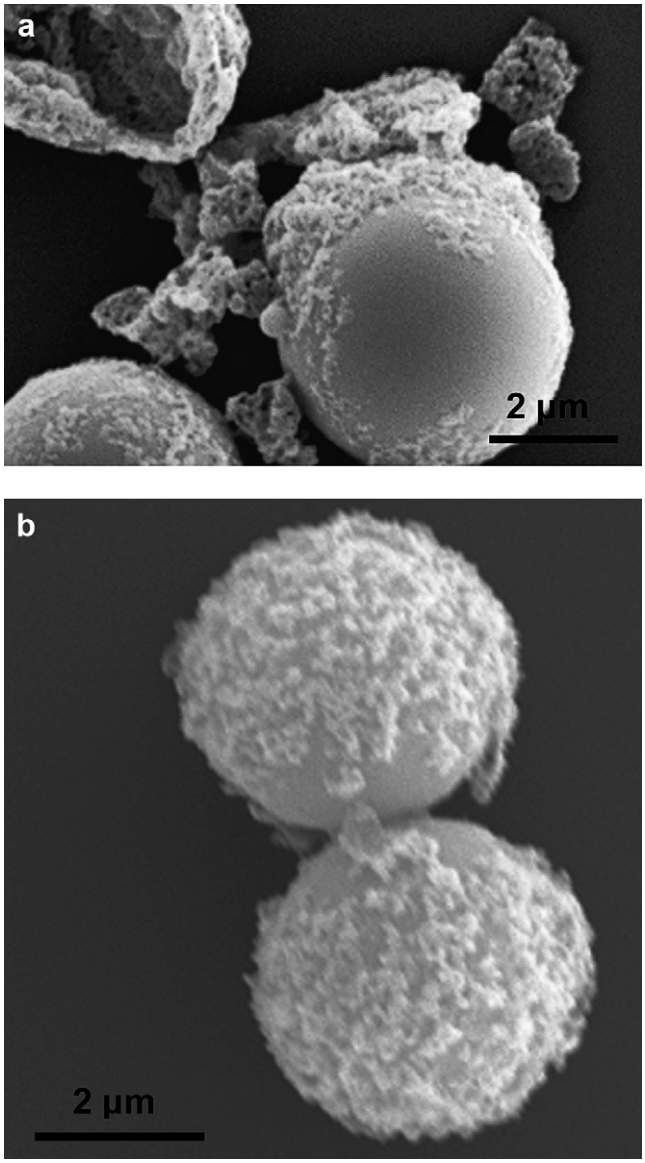

Fig. 6. SEM images of silica particles after the solution-based assembly of four bilayers of PLA nanoparticles with PVPON (a) and with PEI (b).

UV–visible spectra of the PLA SA-LbL films on quartz substrates were recorded using a UV-2450 spectrophotometer (Shimadzu). The dry film thickness was determined using a M-2000U spectroscopic ellipsometer (Woollam).

Surface morphology of the films and shells was examined using atomic force microscopy (AFM) with a Dimension-3000 AFM microscope (Digital Instruments) in the "light" tapping mode according to the established procedure [78]. For film thickness measurements, a scratch was made and height histograms were analyzed. For preparation of a hollow capsule sample, a drop of shells suspension was placed onto a pre-cleaned silicon wafer and dried in air prior to AFM imaging. For shell thickness measurements, the capsule single wall thickness was determined as half of the height of the collapsed flat regions of dried capsules using bearing analysis from NanoScope software to generate height histograms. The PLA or PLA–PEI nanoparticle sizes were determined by measuring the height of individual particles using cross-section analysis of AFM topography images. For the particle height analysis, 40 individual particles for each sample were measured. For average thickness values, the flat regions of 20 microcapsules were analyzed.

Transmission electron microscopy (TEM) was performed on a JEOL 1200EX electron microscope operated at 100 kV. To analyze the PLA nanoparticle films and hollow shells, they were placed on a carbon-coated gold grid (Electron Microscopy Sciences) and dried in air before TEM analysis. For average size of the reduced gold nanoparticles, 15 microcapsules from each sample were analyzed.

3. Results and discussion

3.1. Preparation of PLA nanoparticles

PLA nanoparticles for LbL assembly were prepared using acetone as a solvent for PLA polymer through the nanoprecipitation method [65]. Two types of PLA nanoparticles, bare PLA and PEI-surrounded PLA nanoparticles (further denoted as PEI–PLA) were prepared (Scheme 1). Acetone was removed by evaporation during the preparation process and PLA nanoparticles were formed in the form of colloidal dispersion in aqueous phase [59]. As known, properties of the solvent, such as miscibility with water, diffusion rate to the aqueous outer phase during the nanoprecipitation can affect the properties of the produced particles such as size and stability of the particles in dispersions [79].

Fig. 1 shows topography (left) and phase (right) AFM images, for bare PLA and PLA–PEI nanoparticles prepared in this work (Fig. 1a and b, respectively). As seen, the degree of aggregation for bare PLA nanoparticles is larger as compared to that of PLA–PEI nanoparticles. The possible reason for better dispersed PLA–PEI nanoparticles after being dried on silicon wafer surfaces is the steric and charge stabilization provided by the PEI "shell" around the nanoparticles unlike the terminal carboxylic groups present on surfaces of bare PLA particles (Scheme 1). We suggest that despite PLA deprotonation in de-ionized water (zeta-potential of bare PLA nanoparticles is -40 ± 1 mV at pH = 6.5) and a good stability of the particle dispersion under these conditions, the PLA particles exhibit poor steric stabilization when dried on surfaces and thus aggregate under capillary forces unlike the PLA–PEI particles, which have additional strong steric stabilization due to branched nature of PEI [80,81].

Fig. 2 presents a cross-sectional analysis of areas with the individual particles for two types of the PLA particles and resulting size distributions for the PLA and PLA–PEI nanoparticles (Fig. 2). The average size for bare PLA nanoparticles is slightly larger than that for PLA–PEI nanoparticles, i.e. 50 ± 14 nm and 45 ± 5 nm, respectively, and the size distribution is narrower for the PLA–PEI nanoparticles. These differences can be explained by the fact that addition of water to the PLA polymer solution in acetone during the preparation causes solvent diffusion into the aqueous phase thus forming local polymer super saturation. From these regions, polymer drops are created which further desolvate to produce stable solvent-free particles. The PEI in this case works as a surfactant which hinders coalescence of the droplets thus eventually allowing the formation of smaller PLA–PEI nanoparticles with narrower diameter distribution [82].

3.2. Assembly of PLA nanoparticles via hydrogen-bonding

Scheme 2.1 depicts assemblies of bare PLA nanoparticles with polymers. Bare PLA nanoparticles present a spherical entanglement of the PLA chains with either hydroxyl or carboxylic groups exposed to the aqueous phase (Scheme 3). The hydrogen-bonding-driven assembly of the PLA nanoparticles with PVPON in this case can be realized through the carbonyl moieties of PVPON and terminal carboxylic groups which are presented at the surfaces of PLA nanoparticles under conditions when COOH groups are protonated (Scheme 3 and Scheme 2.1a). We found that the assembly of bare

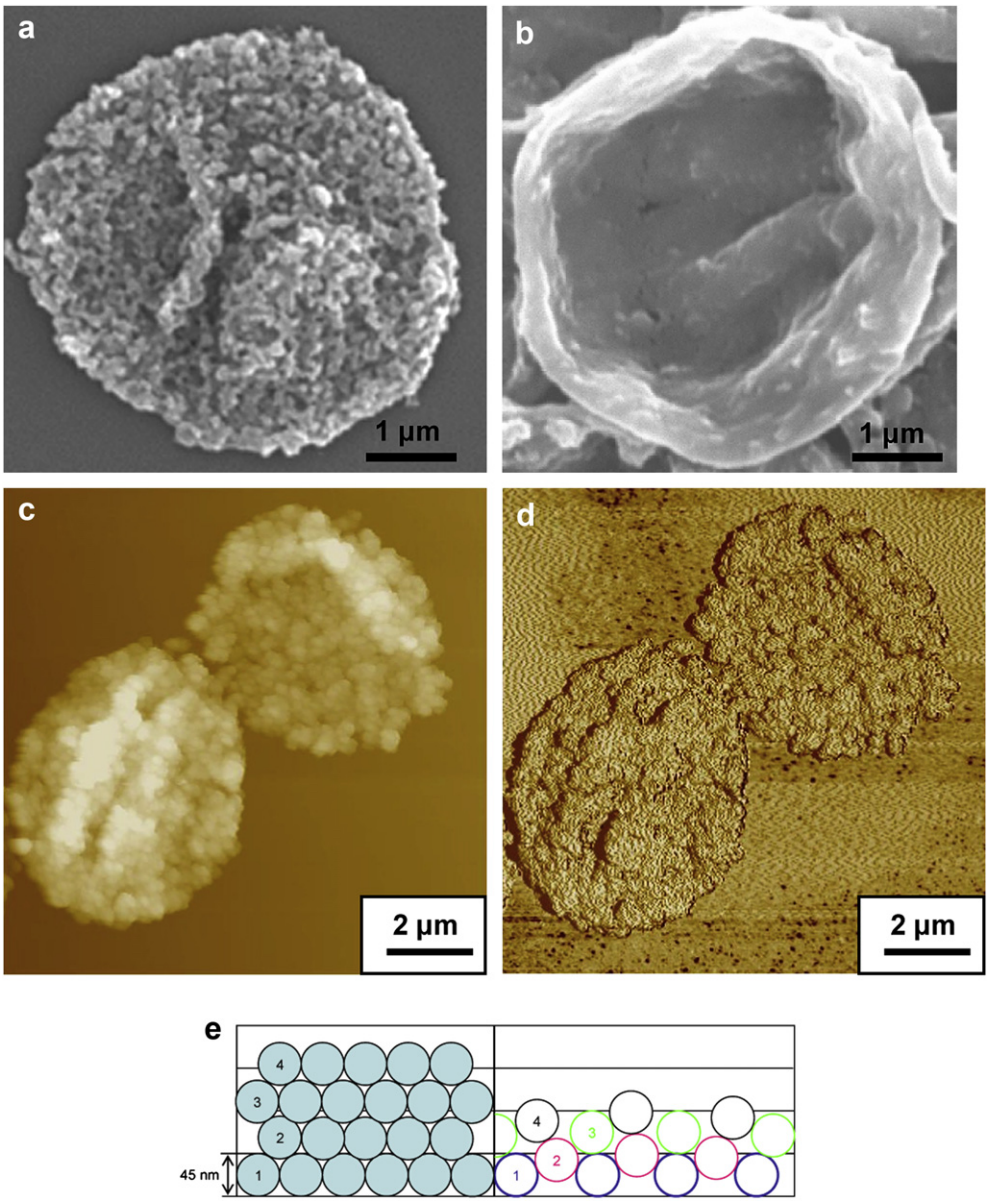

Fig. 7. SEM images of hollow $(PLA–PEI/PAA)_4$ shells assembled from cationic PLA–PEI-0.2 mg/mL nanoparticles (a) and from PLA–PEI-2 mg/mL (b). AFM topographical (c) and phase (d) images of $(PLA–PEI–Au/PAA)_4$ shells made from PLA–PEI-0.2 mg/mL nanoparticles. Schematic representation of the $(PLA–PEI/PAA)_4$ shell structures from ideally (left) and loosely (right) assembled PLA–PEI nanoparticles. Numbers 1,2,3,4 denote a particle layer number (e).

PLA nanoparticles with PVPON was not possible at pH $>$ 2.5 (see film growth data in Fig. 3). Such a limitation on the PVPON/PLA assembly can be explained by the unusually low pK_a value of PLA's carboxylic acid end groups ($pK_a \sim 3.0$) compared to other carboxylic acid groups [83].

At lower pH, the consistent growth for PVPON/PLA films has been observed (Fig. 3a). After the first two bilayers, the overall growth for (PVPON/PLA) was linear with the thickness of approximately 13 nm per a bilayer. This value is smaller than the expected incremental thickness with the PLA particle size of ~45 nm and evidences for incomplete coverage of the substrate surface with the PLA particles as in fact is confirmed by AFM (not shown). However, after seven bilayers, the LbL films with closely packed PLA nanoparticles can be obtained (Fig. 4a and b).

When bare PLA particles were sandwiched in between (PVPON/PAA/PVPON) layers (Scheme 2.1b), the amount of PLA nanoparticles within the film was less than that for (PVPON/PLA) films (Fig. 4c and d). The hypothesis that the PLA particles can assemble into stacks due to the presence of both carboxylic and hydroxyl terminal groups on the PLA particle surfaces was tested and proven invalid [50,59]. Even the surface priming with the first PVPON layer deposited on top of $(PEI/PAA)_2$ pre-layers for better initial adhesion did not result in (PLA/PLA) growth confirming that PLA nanoparticles can not be assembled into stacks through hydrogen-bonding without a polymer counterpart.

The hydrogen-bonded (PVPON/PLA) films exhibited a high pH stability in the range from pH = 2 to pH = 10 which is unusual for the systems assembled only through hydrogen-bonding interactions (Fig. 3b, circles). We attribute such high stability of (PVPON/PLA) films to additional hydrophobic interactions between the PLA nanoparticles. The similar favorable effect of cooperative hydrophobic interactions on stability of hydrogen-bonded layers was reported when PVPON was assembled with more hydrophobic poly (ethacrylic acid) (PEAA) instead of poly(methacrylic acid) when the

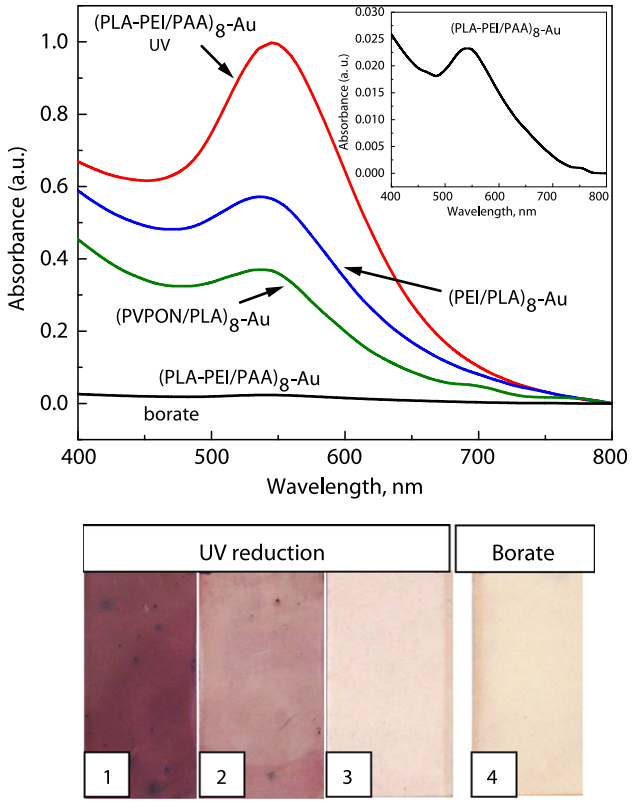

Fig. 8. UV–visible spectra of PLA nanoparticle-based films after gold reduction by UV-irradiation or in borate buffer. Inset shows the UV–vis spectrum from (PLA–PEI–Au/PAA)$_8$ film with gold reduced in borate buffer. Optical images of the gold-containing PLA films: (PLA–PEI/PAA)$_8$ (1), (PEI/PLA)$_8$ (2), (PVPON/PLA)$_8$ (3), (PLA–PEI/PAA)$_8$, (4).

dissolution pH for PVPON/PEAA was almost 4 units of pH higher than the pK_a of PEAA [31]. Indeed, when PLA nanoparticles were sandwiched between (PVPON/PAA/PVPON) layers, the reduced interactions between PLA nanoparticles resulted in the lower pH stability compared to the (PVPON/PLA) (Fig. 3b, squares). These films could be dissolved at pH = 4.6 due to the increased ionization of the poly(acrylic acid) at pH close to the pK_a of PAA ~ 4.5. This dissolution is in good agreement with the previously reported pH stability of PVPON/PAA films [29].

3.3. Assembly of PLA nanoparticles via ionic interactions

To extend the pH range at which the PLA nanoparticle assemblies can be formed, we explored the fabrication of the PLA nanoparticle films through ionic interactions. For that, bare PLA particles were assembled with poly(ethylene imine) (PEI/PLA) and the cationic PLA–PEI particles were stacked with PAA (PLA–PEI/PAA) (Scheme 2.2a and b, respectively). The deposition of the bare PLA nanoparticles was performed at pH 6.8, when the surface carboxylic groups on the particles are fully ionized (pK_a ~ 3).

Fig. 5a demonstrates the growth of PEI/PLA and PLA–PEI/PAA LbL films. Both systems demonstrated linear growth under utilized conditions with the average thickness increase of 20 nm per a bilayer. The observed high average thickness compared to that for the hydrogen-bonding driven assembly can be explained by the fact that PEI has the 60% of its amines protonated at this pH value [84,85]. Thicker films are usually reported when the charge density on the polyelectrolytes is decreased [86]. Also, PEI has a branched architecture and is known to produce thicker films compared to the linear polyelectrolytes [87]. Clearly, the deposition through electrostatic assembly used in this work produced thicker PLA nanoparticle assemblies compared to the hydrogen-bonded PLA nanoparticle films. However, the deposition pH window is narrower for the hydrogen-bonded PLA/PVPON films limiting its fabrication range.

AFM imaging of (PEI/PLA)$_8$ LbL films revealed the presence of aggregated PLA nanoparticles smoothered by the presence of linear counterpart. The micro roughness measured from 1 μm^2 areas was 43 ± 3 nm. This micro roughness value is much higher than those usually observed for linear polyelectrolytes (0.5–3 nm) and for LbL films with embedded nanoparticles (5–10 nm) [88]. The higher roughness of the films can be caused by the fact that solvent is quickly removed in the SA-LbL assembly and the shear forces result in easy agglomeration of the PLA particles due to their low steric stabilization as discussed above. In contrast, when cationic PLA–PEI nanoparticles were employed for the assembly with PAA, the (PLA–PEI/PAA) films were much smoother with the average roughness of 7 ± 2 nm. Clearly, the positively charged "shell" of branched PEI prevented PLA–PEI particles from agglomerating during the SA-LbL deposition due to mutual repulsions of the PEI "shells".

As-prepared, both systems, PEI/PLA and PLA–PEI/PAA, were stable in the tested pH range from 4.5 to 7.5 and did not dissolve (Fig. 5b). However, to render the films stable at extreme pH values, i.e. 3 > pH > 9, when ionization degree of PEI polycations or PAA can change and lead to film destruction, carbodiimide-assisted covalent cross-linking of the films was performed. The exposure of non-cross-linked (PLA–PEI/PAA)$_8$ films to pH = 10 resulted in their 80% mass-loss confirmed by ellipsometry measurements due to pH-induced disassembly which was not observed after the cross-linking of (PLA–PEI/PAA)$_8$ films was performed. Thus, after the cross-linking and introduction of amide linkages between amino groups of the PEI and terminal carboxylic groups of PLA or between the PEI "shell" and PAA, the films stability at basic pH was ensured.

3.4. Assembly of PLA nanoparticle films on silica particles

To understand if the PLA assemblies can be easily applied to various geometrical substrates, we used spherical silica particles as a template material (Scheme 4, steps 1–4). One of the advantages of this approach is that formation of the free-standing coatings as hollow shells can be realized and their properties can be studied regardless of surface effects (Scheme 4, step 8). We found that direct deposition of PVPON/PLA or PEI/PLA stacks on silica surfaces was inhibited (Fig. 6). Taking into account that in these cases the deposition is performed under vigorous shaking, we attribute this inhibition to low mechanical robustness of the (PVPON/PLA) or (PEI/PLA) films. This assumption is also confirmed by the fact that conformal and mechanically robust (PVPON/PLA) or (PEI/PLA) stacks could not be formed even on silica particles pre-modified with (PEI/PAA)$_2$ layers to enhance the adsorption of the following stacks to silica surfaces.

In contrast, tight and self-supporting shells of (PLA–PEI/PAA)$_4$ could be successfully produced after core etching when the cationic PLA nanoparticles were utilized (Fig. 7). We found that the cationic PLA particles synthesized in the presence of 0.2 mg/mL PEI (PLA–PEI-0.2 mg/mL) produce raspberry-like shells unlike those made of (PLA–PEI-2 mg/mL) used for substrate-tethered (PLA–PEI/PAA) coatings (Fig. 7a and b, respectively). We suggest that in the case of (PLA–PEI-2 mg/mL), high concentration of the PEI polymer surfactant results in less PLA nanoparticles adsorbed on the silica surfaces due to preferential interaction between the PEI free polymer chains and PAA. Thus, the 10-fold decrease in the concentration of the PEI polymer surfactant leads to less PEI in solution and much more (PLA–PEI-0.2 mg/mL) particles accessible for assembly.

AFM height analysis on flat regions of (PLA–PEI/PAA)$_4$ shells dried on silicon wafers revealed a single wall thickness of 85 ± 9 nm. Taking into account the average size of PLA–PEI

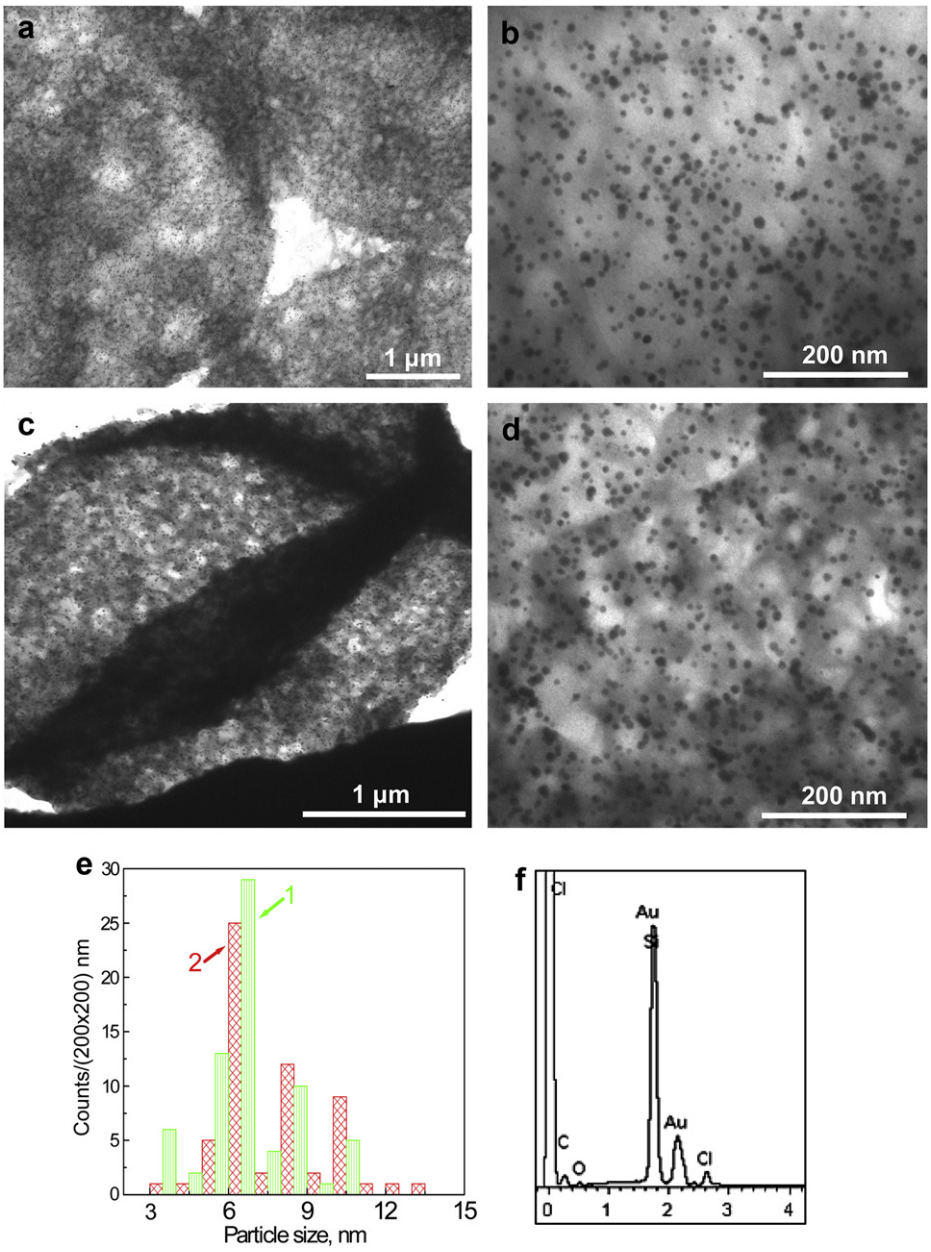

Fig. 9. TEM images of (PLA–PEI–Au/PAA)$_4$ hollow shells after gold reduction in borate buffer. Hollow shells were assembled from cationic PLA–PEI-0.5 mg/mL (a, b) and from PLA–PEI-0.2 mg/mL (c, d) nanoparticles. Histograms of gold nanoparticle size distribution in (PLA–PEI-0.2 mg/mL)/PAA (1) and in (PLA–PEI-0.5 mg/mL)/PAA (2) systems (e). EDX spectrograph of hollow (PLA–PEI-0.2 mg/mL-Au/PAA)$_4$ shells (f).

nanoparticle being 45 nm and a thickness of the (PEI/PAA)$_2$ prelayer of 6 ± 2 nm, it is clear that produced nanoshells possess a loosely packed nanoparticle structure as schematically shown in Fig. 7. The loosely packed structure shown on the right is adopted, presumably due to the voids between the adsorbed PLA–PEI nanoparticles which are, in turn, formed because of the stabilizing PEI "shell" around the cationic PLA particles preventing them from close arrangements.

3.5. Gold nanoparticles growth inside the PLA nanoparticle coatings

To produce thin films capable of an optical report of film degradation, we pursued gold reduction in the PLA nanoparticle films. In our recent work, we have demonstrated that gold nanoparticles can be grown within hydrogel LbL films by reduction of $[AuCl_4]^-$ ions bound to free amine groups present in the polymer matrix due to ethylene diamine crosslinker [64]. Therefore, gold nanoparticles were grown within the PLA nanoparticle films by reducing $[AuCl_4]^-$ ions which were allowed to penetrate inside the films and form ionic pairs with protonated amine groups. After non-interacted tetrachloroaurate ions were rinsed away by the buffer solution, gold reduction was performed by two methods, i.e. either using UV-irradiation or under mild reducing conditions of borate buffer at pH 10 (see Experimental; Scheme 4, steps 5–7) [63,64].

Fig. 8 demonstrates UV–visible spectra of the PLA nanoparticle films after gold reduction. Fig. 8-1 and 8-2 shows optical images of the 8-bilayer (PLA–PEI/PAA) and (PEI/PAA) films after gold reduction upon UV-irradiation. The amount of gold nanoparticles decreased from (PLA–PEI/PAA)$_8$ to (PEI/PLA)$_8$ systems. All studied

systems exhibit a distinctive band at~550 nm which corresponds to surface plasmon resonance from gold nanoparticles [89]. The higher intensity of the gold peak in $(PLA–PEI/PAA)_8$ suggests higher content of gold nanoparticles within these layers. This can be explained by higher concentration of amine groups in the PEI "shell" around the PLA particles presumably due to larger surface area of PLA–PEI compared to that of a PLA nanoparticle layer exposed to PEI during the assembly (spectra in Fig. 8).

The $(PVPON/PLA)_8$ system was also studied for its ability to reduce gold. To achieve that, free amine groups were introduced into the film using ethylene diamine molecules [64]. For that, terminal carboxylic groups on PLA particles within the film were activated with carbodiimide and reacted with ethylene diamine [64]. The absorbance peak appears at 538 nm for the $(PVPON/PLA)_8$ modified with EDA (Fig. 8, spectrum and Fig. 8-3). However, the observed SPR peak from gold for (PVPON/PLA) film had a lower intensity compared to that of ionic PLA nanoparticle assemblies suggesting much lower amount of available amine groups in the modified (PLA–Au/PVPON) film.

The presence of gold nanoparticles after reduction in borate buffer at pH = 10 was also confirmed by the emerging SPR band in the UV–visible spectrum (Fig. 8, inset). The lower concentration of gold nanoparticles can be seen from comparison of light absorption levels for $(PLA–PEI/PAA)_8$ films reduced via the UV-irradiation and in the borate buffer. Such a decrease can be due to high pH conditions of the borate buffer method where the amount of available protonated amine groups in PEI is significantly reduced (pK_a values for primary amines of PEI is 9.5 respectively) [84] (Fig. 8-1 and 8-4, respectively). The UV-assisted gold reduction, however, resulted in dramatic agglomeration of the treated shells which were mostly damaged and impossible to re-disperse after the UV treatment. In contrast, the $(PLA–PEI\text{-}0.2\ mg/mL/PAA)_4$ shells kept their raspberry-like surface morphology after gold nanoparticles were reduced within the shells in borate buffer (Fig. 7c) Importantly, the shell integrity was preserved after such treatment (Fig. 7d).

The dimensions of gold nanoparticles can be estimated from the absorption peak position [90]. It has been reported that the increase of the nanoparticle size results in a red-shift, and the broader size distribution should result in peak broadening [89]. The spectra were analyzed by using Lorenzian fitting to obtain the peak position. The estimation of the average gold particle size reduced within the planar assemblies by the peak position and its half-width using the data for spherical gold nanoparticles reported previously gave diameter below 40 nm [89–92]. This estimation is consistent with the data from TEM analysis of the gold nanoparticles within the $(PLA–PEI–Au/PAA)_4$ shells. Fig. 9 shows TEM analysis of the $(PLA–PEI–Au/PAA)_4$ hollow capsules with clear evidence of the reduced gold nanoparticles within the coatings. Gold reduction in both systems either formed from PLA–PEI-0.2 mg/mL or from PLA–PEI-0.5 mg/mL nanoparticles, resulted in fine gold nanoparticles of a similar size (7±3 nm and 6 ± 3 nm, respectively, Fig. 9e). The EDX spectrograph additionally confirms the presence of gold nanoparticles (Fig. 9f).

3.6. Enzymatic degradation of the PLA nanoparticle coatings and its colorimetric report

Recently, LBL shells with gold nanoparticles deposited inside the film were demonstrated to deliver microcapsule inner contents upon the temperature change of gold nanoparticles on resonance with an excitation source [91–93]. In this work we studied enzymatic degradation of the PLA nanoparticle assemblies in the presence of α-chymotrypsin and utilized reduced gold nanoparticles as optical reporters for the biodegradation process. As known,

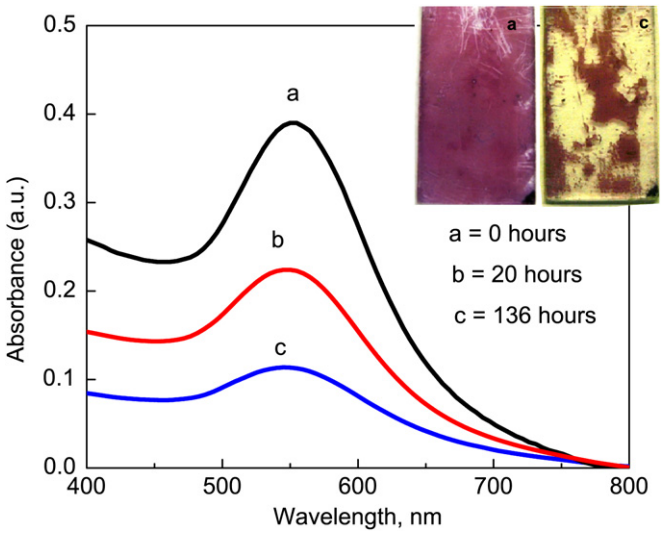

Fig. 10. UV–visible spectra of the $(PLA–PEI–Au/PAA)_8$ quartz-tethered film after its exposure to α-chymotrypsin solution at pH = 7.5 (36 °C) for various times. Inset shows optical images of the $(PLA–PEI–Au/PAA)_8$ film after 0 (a) and 136 (c) hours of exposure to the enzymatic solution.

α-chymotrypsin is the most suitable serine protease enzyme that hydrolyzes PLA [77]. Besides, α-chymotrypsin was chosen because of its activity in the human stomach, and its ability to degrade composite PLA assemblies is important for potential biomedical applications.

Fig. 10 shows the UV–visible spectrum from the $(PLA–PEI–Au/PAA)_8$ film before its exposure to α-chymotrypsin solution (Fig. 10a). The SPR signal from gold nanoparticles within the PLA nanoparticle assemblies observed at around 550 nm can be utilized to monitor the biodegradation process. The $(PLA–PEI–Au/PAA)_8$ films exposed to acidic and basic aqueous solutions without enzyme did not show any changes in the SPR peak intensity. The diminished SPR intensity from the film was observed after the film exposure to the buffer solution in the presence of α-chymotrypsin at 36 °C (pH = 7.5) for 20 or 136 h thus showing high sensitivity of the optical approach to report film degradation (Fig. 10b, c). As suggested, the degradation of the PLA assembly is achieved by disruption of the amide linkages between PEI and PAA components of the assembly as well as breakage of the ester bonds in the PLA nanoparticles by α-chymotrypsin via surface erosion mechanism [94]. The relatively slow kinetics of tens of hours might be due to the slow diffusion of α-chymotrypsin limited by strong interactions between the adjacent layers inside the film or due to possible inhibitory effects of PEI towards the enzyme [77]. We suggest that the decoration of PLA nanoparticles with fine gold nanoparticles is critical for observation of dramatic changes in film optical properties observed in the course of PLA nanoparticles biodegradation. Considering the sensitivity and easy monitoring routine of this approach in comparison to conventional mass-loss testing, we believe that the self-reporting design proposed here can be readily employed for real-time colorimetric report of biodegradation processes within ultra-thin polymer films.

4. Conclusions

We demonstrated the assembly of biodegradable PLA nanoparticles into robust thin multilayer films followed by their optically monitored biodegradation. The PLA nanoparticles of 50 ± 20 nm were prepared from high molecular weight PLA by controlled precipitation from acetone and integrated into the

ultra-thin films using tailored hydrogen-bonding ability or ionic interactions. Narrower PLA nanoparticle size distribution can be obtained by co-precipitation of PLA with PEI, which results in the stable cationic nanoparticles thus facilitating the ionically-driven assembly with poly(acrylic acid). On the other hand, hydrogen-bonded assemblies of PVPON/PLA pairs possess a unique pH-stability in the broad pH range from pH = 2 to pH = 10, possibly, due to additional hydrophobic interactions between PLA particles and limited steric stabilization at the particle surfaces. In contrast to planar assemblies, only PLA–PEI particles were possible to assemble into conformal coatings through ionic interactions on silica particles to yield free-standing hollow shells of $(PLA–PEI/PAA)_n$.

Finally, to design a facile optical reporting tool for biodegradation processes, gold nanoparticles were successfully grown within the PLA nanoparticle-based films due to the present amine groups. These in-situ grown gold nanoparticles can be utilized as optical nano-reporters for colorimetric monitoring of biodegradation process within the thin films in the presence of α-chymotrypsin with high sensitivity. We suggest that these nanocomposite and ultra-thin PLA nanoparticle layered films can find use in bionanotechnology and biomedical applications which require simple, facile, and real-time monitoring of biodegradation processes.

Acknowledgements

We thank the National Science Foundation, award NSF-CBET-NIRT 0650705 (V.K. and V.V.T) the Air Force Office of Scientific Research (FA9550-08-1-0446 project) (E.K. and V.V.T.), COLCIENCIAS and the Universidad de Antioquia, Colombia (V.H.O. and B.L.L.) for financial support. We are grateful to the Colciencias Program "Apoyo a la comunidad científica nacional a través de doctorados nacionales 2005" (V.H.O.).

References

[1] Hall DB, Underhill P, Torkelson JM. Polym Eng Sci 1998;38(12):2039–45.
[2] Miller AF. Science 2007;317(5838):605–6.
[3] Rotella C, Napolitano S, Wulbbenhorst M. Macromolecules 2009;42(5):1415–7.
[4] Tsukruk VV. Prog Polym Sci 1997;22(2):247–311.
[5] Pérez LD, López JF, Orozco VH, Kyu T, López BL. J Appl Polym Sci 2009;111(5):2229–37.
[6] Vargas AF, Brostow W, Hagg Lobland HE, Lopez BL, Olea-Mejia O. J Nanosci Nanotechnol 2009;9:6661–7.
[7] Zou H, Wu S, Shen J. Chem Rev 2008;108(9):3893–957.
[8] Jiang C, Markutsya S, Pikus Y, Tsukruk VV. Nat Mater 2004;3(10):721–8.
[9] Jiang C, Markutsya S, Shulha H, Tsukruk VV. Adv Mater 2005;17(13):1669–73.
[10] Jiang C, McConney ME, Singamaneni S, Merrick E, Chen Y, Zhao J, et al. Chem Mater 2006;18(11):2632–4.
[11] Jiang C, Tsukruk VV. Adv Mater 2006;18(7):829–40.
[12] Lin YH, Jiang C, Xu J, Lin Z, Tsukruk VV. Adv Mater 2007;19(22):3827–32.
[13] Zimnitsky D, Jiang C, Xu J, Lin Z, Zhang L, Tsukruk VV. Langmuir 2007;23(20):10176–83.
[14] Zimnitsky D, Shevchenko VV, Tsukruk VV. Langmuir 2008;24(12):5996–6006.
[15] Brauman JI, Szuromi P. Science 1996;273(5277):855.
[16] Hong J, Lowack K, Schmitt J, Decher G. Layer-by-layer deposited multilayer assemblies of polyelectrolytes and proteins: from ultrathin films to protein arrays. Trends in Colloid and Interface Science 1993;VII:98–102.
[17] Lin YH, Jiang C, Xu J, Lin ZQ, Tsukruk VV. Soft Matter 2007;3(4):432–6.
[18] Lvov Y, Ariga K, Ichinose I, Kunitake T. J Am Chem Soc 1995;117(22):6117–23.
[19] Berger S, Zhang H, Pich A. Adv Funct Mater 2009;19(4):554–9.
[20] Li J, Liu B, Li J. Langmuir 2005;22(2):528–31.
[21] Zhang G, Wang D, Gu Z-Z, Hartmann J, Mohwald H. Chem Mater 2005;17(21):5268–74.
[22] Zhang J, Xu S, Kumacheva E. Adv Mater 2005;17(19):2336–40.
[23] Decher G, Schlenoff JB. Multilayer thin films. Weinheim: Wiley-VCH; 2003.
[24] Decher G, Hong JD. Makromolekulare Chemie-Macromolecular Symposia 1991;46:321–7.
[25] Gunawidjaja R, Ko H, Jiang C, Tsukruk VV. Chem Mater 2007;19(8):2007–15.
[26] Decher G. Science 1997;277(5330):1232–7.
[27] Decher G, Hong JD. Berichte Der Bunsen-Gesellschaft-Physical Chemistry Chemical Physics 1991;95(11):1430–4.
[28] Kharlampieva E, Kozlovskaya V, Sukhishvili SA. Adv Mater 2009;21(30):3053–65.
[29] Kharlampieva E, Sukhishvili SA. Polym Rev 2006;46(4):377–95 (Philadelphia, PA, U.S.).
[30] He Q, Möhwald H, Li J. Macromol Rapid Commun 2009;30(18):1538–42.
[31] Kozlovskaya V, Shamaev A, Sukhishvili SA. Soft Matter 2008;4(7):1499–507.
[32] Kozlovskaya V, Kharlampieva E, Drachuk I, Cheng D, Tsukruk VV. Soft Matter; 2010; doi:10.1039/b927369g.
[33] Tang Z, Wang Y, Podsiadlo P, Kotov NA. Adv Mater 2006;18(24):3203–24.
[34] Srivastava S, Kotov NA. Acc Chem Res 2008;41(12):1831–41.
[35] Kumar M, Kumar N, Domb A, Arora M. Pharmaceutical polymeric controlled drug delivery systems. Filled elastomers drug delivery systems; 2002. p. 45–117
[36] Kong W, Zhang X, Gao ML, Zhou H, Li W, Shen JC. Macromol Rapid Commun 1994;15(5):405–9.
[37] Erel-Unal I, Sukhishvili SA. Macromolecules 2008;41(11):3962–70.
[38] Caruso F, Niikura K, Furlong DN, Okahata Y. Langmuir 1997;13(13):3422–6.
[39] Caruso F, Lichtenfeld H, Giersig M, Mohwald H. J Am Chem Soc 1998;120(33):8523–4.
[40] Wei X, Gong C, Gou M, Fu S, Guo Q, Shi S, et al. Int J Pharm 2009;381(1):1–18.
[41] Nouvel C, Raynaud J, Marie E, Dellacherie E, Six JL, Durand A. J Colloid Interface Sci 2009;330(2):337–43.
[42] Meng F, Hennink WE, Zhong Z. Biomaterials 2009;30(12):2180–98.
[43] Cheng J, Wang J. Sci China Ser B Chem 2009;52(7):961–8.
[44] Wong SY, Pelet JM, Putnam D. Prog Polym Sci 2007;32(8–9):799–837.
[45] Pinto Reis C, Neufeld RJ, Ribeiro AJ, Veiga F. Nanomedicine: Nanotechnology, Biol Med 2006;2(1):8–21.
[46] Orozco VH, Witold B, Chonkaew W, López BL. Macromol Symp 2009;277(1):69–80.
[47] Orozco VH, Vargas AF, López BL. Macromol Symp 2007;258(1):45–52.
[48] Helle A, Hirsjärvi S, Peltonen L, Hirvonen J, Wiedmer SK. J Chromatogr A 2008;1178(1–2):248–55.
[49] de Faria TJ, de Campos AM, Senna EL. Macromol Symp 2005;229(1):228–33.
[50] Nobs L, Buchegger F, Gurny R, Allémann E. Eur J Pharm Biopharm 2004;58(3):483–90.
[51] Lim JY, Hansen JC, Siedlecki CA, Hengstebeck RW, Cheng J, Winograd N, et al. Biomacromolecules 2005;6(6):3319–27.
[52] Ding AG, Shenderova A, Schwendeman SP. J Am Chem Soc 2006;128(16):5384–90.
[53] Zavan B, Vindigni V, Vezzù K, Zorzato G, Luni C, Abatangelo G, et al. J Mater Sci Mater Med 2009;20(1):235–47.
[54] Trimaille T, Pichot C, Elaïssari A, Fessi H, Briançon S, Delair T. Colloid Polym Sci 2003;281(12):1184–90.
[55] Stainmesse S, Orecchioni AM, Nakache E, Puisieux F, Fessi H. Colloid Polym Sci 1995;273(5):505–11.
[56] Moinard-Chécot D, Chevalier Y, Briançon S, Beney L, Fessi H. J Colloid Interface Sci 2008;317(2):458–68.
[57] Allémann E, Leroux J-C, Gurny R, Doelker E. Pharm Res 1993;10(12):1732–7.
[58] Ogawa Y, Arikawa Y, Kida T, Akashi M. Langmuir 2008;24(16):8606–9.
[59] Hirsjarvi S, Peltonen L, Hirvonen J. Colloids Surf B Biointerfaces 2006;49(1):93–9.
[60] Jiang C, Tsukruk VV. Soft Matter 2005;1(5):334–7.
[61] Gorin DA, Portnov SA, Inozemtseva OA, Luklinska Z, Yashchenok AM, Pavlov AM, et al. Phys Chem Chem Phys 2008;10(45):6899–905.
[62] Bedard MF, Munoz-Javier A, Mueller R, Pd Pino, Fery A, Parak WJ, et al. Soft Matter 2009;5(1):148–55.
[63] Chia K-K, Cohen RE, Rubner MF. Chem Mater 2008;20(21):6756–63.
[64] Kozlovskaya V, Kharlampieva E, Chang S, Muhlbauer R, Tsukruk VV. Chem Mater 2009;21(10):2158–67.
[65] Fessi H, Puisieux F, Devissaguet JP, Ammoury N, Benita S. Int J Pharm 1989;55(1):R1–4.
[66] Seo J, Lutkenhaus JL, Kim J, Hammond PT, Char K. Langmuir 2008;24(15):7995–8000.
[67] Cho J, Char K, Hong JD, Lee KB. Adv Mater 2001;13(14):1076–8.
[68] Harris JJ, DeRose PM, Bruening ML. J Am Chem Soc 1999;121(9):1978–9.
[69] Kozlovskaya V, Kharlampieva E, Mansfield ML, Sukhishvili SA. Chem Mater 2006;18(2):328–36.
[70] Tomita K, Nakajima T, Kikuchi Y, Miwa N. Polym Degrad Stab 2004;84(3):433–8.
[71] Tokiwa Y, Calabia BJ. Polym Environ 2007;15(4):259–67.
[72] Tokiwa Y, Calabia B. Appl Microbiol Biotechnol 2006;72(2):244–51.
[73] Reeve MS, McCarthy SP, Downey MJ, Gross RA. Macromolecules 2002;27(3):825–31.
[74] MacDonald RT, McCarthy SP, Gross RA. Macromolecules 1996;29(23):7356–61.
[75] Kunioka M, Ninomiya F, Funabashi M. Polym Degrad Stab 2006;91(9):1919–28.
[76] Amnat J, Hardaning P, Yutaka T. Macromol Biosci 2002;2(9):420–8.
[77] Lim H-A, Raku T, Tokiwa Y. Biotechnol Lett 2005;27(7):459–64.
[78] Tsukruk VV. Rubber Chem Technol 1997;70(3):430–67.
[79] Galindo-Rodriguez S, Allémann E, Fessi H, Doelker E. Pharm Res 2004;21(8):1428–39.
[80] Tohver V, Smay JE, Braem A, Braun PV, Lewis JA. Proc Natl Acad Sci U S A 2001;98(16):8950–4.
[81] Liu J, Luijten E. Phys Rev Lett 2004;93(24):247802.

[82] Desgouilles SP, Vauthier C, Bazile D, Vacus JL, Grossiord J-L, Veillard M, et al. Langmuir 2003;19(22):9504–10.
[83] Henton DE, Gruber P, Lunt J, Randall J. Polylactic acid technology. In: Mohanty AK, Misra M, Drzal LT, editors. Natural fibers, biopolymersand biocomposites. Boca Raton: CRC Press; 2005. p. 527–77.
[84] Tsuchida E, Nishikawa H. J Polym Sci Polym Chem Ed 1976;14(6):1557–60.
[85] Tong W, Gao C, Mohwald H. Macromolecules 2005;39(1):335–40.
[86] Choi J, Rubner MF. Macromolecules 2004;38(1):116–24.
[87] Erol M, Du H, Sukhishvili S. Langmuir 2006;22(26):11329–36.
[88] Ko H, Jiang C, Tsukruk VV. Chem Mater 2005;17(22):5489–97.
[89] Link S, El-Sayed MA. J Phys Chem B 1999;103(21):4212–7.
[90] Bogatyrev V, Dykman L, Khlebtsov B, Khlebtsov N. Opt Spectrosc 2004;96(1):128–35.
[91] Kreft O, Skirtach AG, Sukhorukov GB, Möhwald H. Adv Mater 2007;19(20):3142–5.
[92] Johnston APR, Cortez C, Angelatos AS, Caruso F. Curr Opin Colloid Interface Sci 2006;11(4):203–9.
[93] del Mercato LL, Rivera-Gil P, Abbasi AZ, Ochs M, Ganas C, Zins I, et al. Nanoscale 2010;2(4):458–67.
[94] Tsuji H, Miyauchi S. Polymer 2001;42(9):4463–7.